Cross-Validation of PLIF and BBLIF towards the Detailed Study of Gas-Sheared Liquid Films in Downward Annular Flows

A.V. Cherdantsev[1,2,3], J.S. An[1], A. Charogiannis[1], C.N. Markides[1,*]
1: Clean Energy Processes (CEP) Laboratory, Department of Chemical Engineering, Imperial College London, UK
2: Laboratory of Transfer Processes, Department of Multiphase Systems, Kutateladze Institute of Thermophysics, Russia
3: Laboratory of High Energy Thermal Processes, Novosibirsk State University, Russia
* Correspondent author: c.markides@imperial.ac.uk

Keywords: Annular flows, Liquid films, Waves, PLIF, BBLIF

ABSTRACT

This paper is devoted to the development and application of two spatiotemporally resolved optical techniques capable of liquid film thickness measurements in downward annular (co-current) gas-liquid flows, namely Planar Laser-Induced Fluorescence (PLIF) and Brightness-Based Laser-Induced Fluorescence (BBLIF). A single laser sheet is used to excite the liquid film, which has been doped with a fluorescent dye, along a longitudinal/vertical plane normal to the pipe wall. Two cameras (one for each technique) are placed at different angles to the plane of the laser sheet in order to recover independently the shape of the gas-liquid interface along this section. The effect of the angle between the laser sheet and the PLIF camera axis is also investigated. It is found that, at film regions where the gas-liquid interface is smooth, the conventional approach used for interpreting PLIF data is vulnerable to total internal reflection of the fluorescent light at the free surface, which leads to an overestimation of the film thickness that increases as the angle between the laser sheet and the camera axis is decreased. Nonetheless, local features such as light intensity maxima or minima can often be located within the fluorescent signal that correctly identify the interface, which in these conditions also coincides with the BBLIF film-thickness measurement. The BBLIF measurement, on the other hand, can lead to localized overestimation of the film thickness at flow regions with significant wave activity, i.e. steep slopes or agitated films, and around gas bubbles entrained into the liquid film, or an underestimation inside the gas bubbles. Correction procedures are developed to compensate distortions caused by both methods that would make these techniques more accurate for standalone employment. The simultaneous application of both techniques is highly recommended to attain the most reliable information.

1. Introduction

Gas-sheared downward annular flows comprise a thin liquid film flowing along the inner circumference of a pipe and a gas core. The film surface is populated by a multiscale system of waves in which large ‘disturbance’ waves dominate, owing to their large amplitudes, lifetimes, longitudinal sizes and velocities. These waves are separated by a much thinner ‘base film’, with smaller ripple waves propagating over both the disturbance waves and the base film. The

experimental investigation of this complex wavy structure is particularly challenging, owing to the intermittent nature of the moving and wavy gas-liquid interface, and the large dynamic range and high spatial and temporal resolution that are required in order to capture the broad range of length and time-scales that are encountered in these flows. A number of measurement techniques have been developed or adapted towards the detailed spatiotemporal characterization of annular gas-liquid flows, including conductivity probes (see, for example, Chu & Dukler 1974; Belt et al. 2010; Karapantsios et al. 1989 and Han et al. 2006), high-speed visualization (see, for example, Woodmansee & Hanratty 1969, and Pham et al. 2014) and the laser focus displacement technique (Hazuku et al. 2008). However, these techniques do not always provide quantitative information on the thickness of the film, are often limited to point measurements, may suffer from low spatial resolution and may disturb the flow.

Two relatively popular and well-suited candidates can be found in the literature for performing detailed quantitate measurements in such flows, both of which are variations of laser-induced fluorescence (LIF) imaging. The first approach is known as Planar LIF or PLIF, and involves the illumination of a section of the flow using a laser sheet, and the measurement of the thickness of the film by identifying the two liquid boundaries (i.e., the gas-liquid and solid-liquid interfaces) in the emitted fluorescence images. Recent applications of PLIF in gas-liquid flows include the work of Schubring et al. (2010), Farias et al. (2012), Zadrazil et al. (2014), Charogiannis et al. (2015) and Charogiannis et al. (2017). The other LIF approach is known as Brightness-Based LIF or BBLIF, and relates the emitted fluorescence-intensity to the film thickness measurement according to the Beer-Lambert law. This method was originally developed for point measurements (see, for example, Hewitt et al. 1964), but was later adapted for two and even three-dimensional measurements (see, for example, Liu et al.1993; Adomeit & Renz 2000; Alekseenko et al. 2005; Kharlamov et al. 2015; Alekseenko et al. 2009; Alekseenko et al. 2014; Cherdantsev et al., 2014; Cherdantsev et al., 2017).

In this work, the wavy structure of gas-liquid annular flows is investigated by simultaneous application of the PLIF and the BBLIF, which allows us to assess the performance of the two techniques in different flow regimes displaying different features (for example, smooth and rough films, steep interfaces and bubbles). The main goal of this contribution is to thoroughly (and quantitatively) examine the shortcomings of the two techniques.

2. Experimental methodology

Optical measurements were conducted in an air-sheared downward annular flow of water in a vertical round pipe of inner diameter D = 32.4 ± 0.4 mm and length ≈ 5 m. The pipe was constructed of FEP as it matches closely the refractive index of water at ambient conditions (n_{FEP} = 1.334 and n_{water} = 1.333). The water flow was introduced into the test section by employment of a conical injector in order to generate circumferentially uniform liquid films (Zhao et al., 2013). The Reynolds number of the gas phase, $Re_G = 4Q_G/\pi D\nu_G$, varied from 0 to 85,100, which corresponds to superficial gas velocities in the range V_G = 0 – 40 m/s. The liquid Reynolds number (defined as $Re_L = Q_L/\pi D\nu_L$) varied in the range Re_L = 150 – 1,350. All measurements were performed at a distance 100 D downstream of the inlet.

A frequency-doubled Nd:YAG laser (532 nm) was used to excite the fluorescent dye, Rhodamine 6G, at a rate of 100 Hz, while a pair of CMOS cameras equipped with Sigma 105 mm f/2.8 macro lenses and 540 nm long-pass filters collected the emitted fluorescence. The BBLIF camera was set at an angle of 15 ° relative to the excitation plane, while the PLIF camera was set either at 90 ° or 70 ° (see Fig. 1). The observation angle was varied in the case of PLIF in order to assess its influence on the film thickness measurement. Hence, two sets of experiments were performed, referred to as PLIF90 and PLIF70. The length of the flow region overlapping the PLIF and BBLIF imaging domains was 34.3 mm for the PLIF90 and 31.5 mm for the PLIF70 experiments. The resulting spatial resolution of the BBLIF- and PLIF-based measurements varied from 26.7 to 30.6 μm/pixel.

The extraction of film-thickness data, in the case of BBLIF, stems from the integration of the Beer-Lambert law (see, for example, Alekseenko et al. (2014),

$$J(x) = C(x)\left[1 - \exp\left(-\alpha h_{BB}(x)\right)\right]\left[1 + K\exp\left(-\alpha h_{BB}(x)\right)\right] \qquad (1)$$

where $J(x)$ is the measured fluorescence intensity, $C(x)$ is a compensation matrix, α is the absorption coefficient of the laser light through the liquid, K is the reflection coefficient of the laser light at the water-air interface ($K \approx 0.02$ when this is flat) and $h_{BB}(x)$ is the film thickness. The compensation matrix, which is used to address the non-uniform energy distribution along the sheet, is calculated from the reference signal, $J_0(x)$, emitted by a liquid film of known thickness, h_0. This was obtained in situ by approximating a Nusselt flow. When the slope of the interface is small (i.e., when $K \approx 0.02$), the measurement error is mainly determined by the camera noise, the non-uniform sensitivity of the sensor and the pulse-to-pulse variation of the laser, and is estimated at up to 10 % for the present BBLIF experiments.

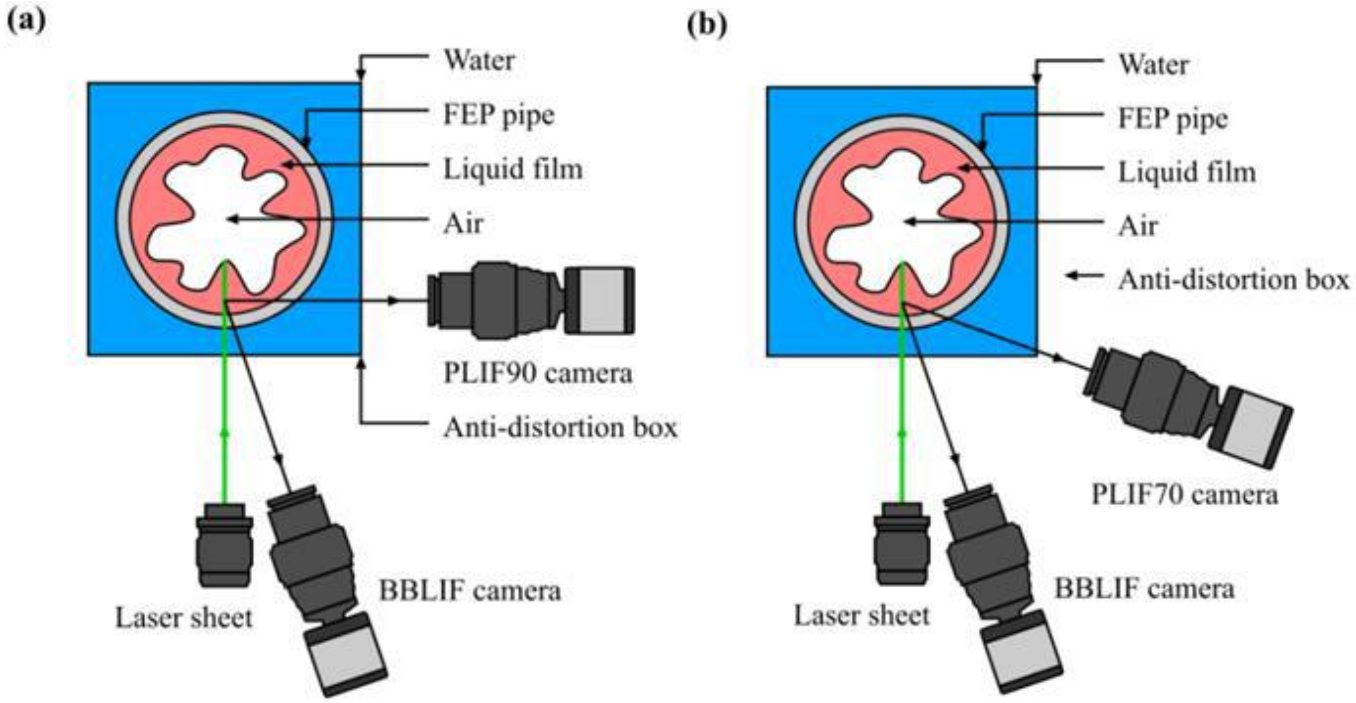


Fig. 1 Experimental configurations of: (a) simultaneous BBLIF and PLIF at 90º (PLIF90), and (b) BBLIF and PLIF at 70 º (PLIF70).

The film-thickness measurement by application of PLIF requires the identification of the two interfaces, gas-liquid and solid-liquid, directly from the PLIF images. In this study, the former was identified from the graticule images (camera calibration images), while the latter was retrieved from each-image column based on an intensity-threshold approach, also using the slope of the interface as an auxiliary criterion. The threshold was set to the arithmetic mean of the maximum and minimum brightness in each column of each raw PLIF-image. The raw PLIF images were binarized using this threshold, and closed morphologically to dampen the effect of random noise. Additional steps were undertaken in order to eliminate out-of-plane features, and also to remove discontinuities at the borders of bubbles entrained in the liquid film.

3. Results and discussion

3.1. Wave regimes

Webb & Hewitt (1975) identified four main wave regimes in downward annular flows, namely "ripples", "dual waves", "thick ripples" and "regular disturbance waves". The transition from the dual-wave to the regular disturbance-wave regime is the most relevant to this study, and can be described by the PLIF frames provided in Fig. 2, which shows three flows with the same Re_L (=

290) but different Re_G. In each sub-figure, the left-hand side shows raw BBLIF images rescaled along the longitudinal coordinate to match the PLIF70 images shown to their right. The latter also include the location of the gas-liquid interface based on BBLIF (red line). The differences between the three cases are easy to identify: for Re_G = 34,600 there are no bubbles and the interface is smooth (the deviations between the PLIF and BBLIF data are discussed later in this paper); for Re_G = 43,200 some large bubbles appear inside the film and the interface becomes more rough, whereas for Re_G = 51,800 the number of bubbles increases sharply, as does the interfacial roughness.

The examination and comparative assessment of PLIF and BBLIF results is henceforth split between "smooth" and "rough" films, as these represent the two main interface patterns observed in the investigated range of flow conditions. The former includes film flows in the absence of gas shear or in the presence of a weak shear, while the latter relates to the emergence of disturbance waves, liquid entrainment in the gas phase and the entrapment of bubbles in the film.

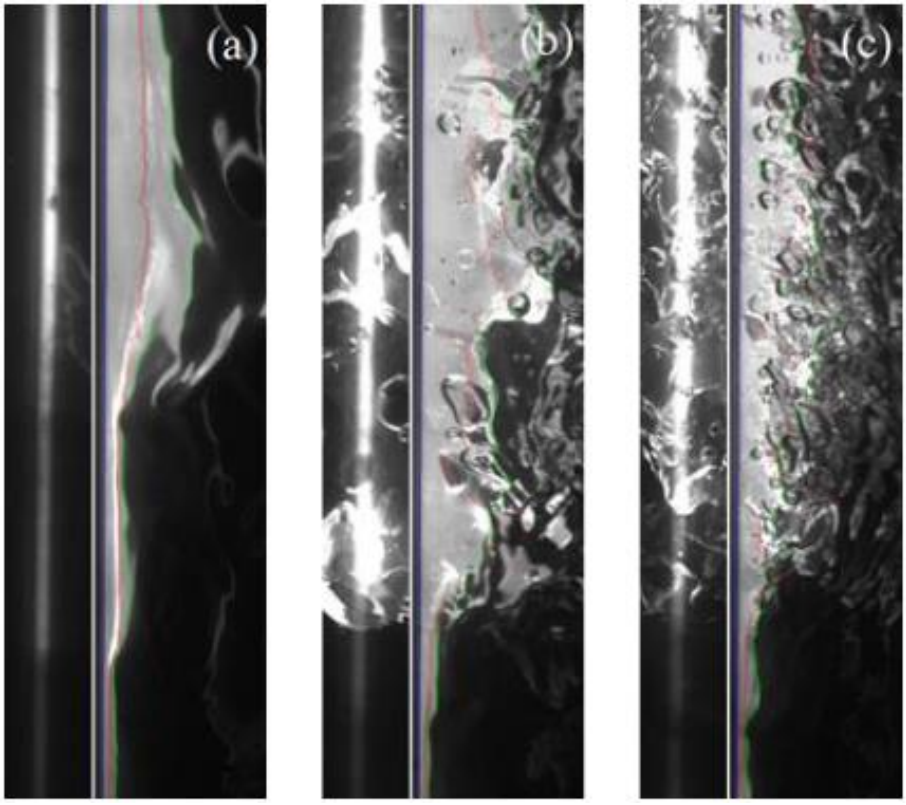


Fig. 2 Raw BBLIF and PLIF70 images from flows with Re_L = 290, and: (a) Re_G = 34,600, (b) Re_G = 41,200, and (c) Re_G = 51,800. The blue line marks the position of the wall, the green line marks the gas-liquid interface obtained by PLIF70, and the red line the same interface obtained by BBLIF.

3.2. Smooth films

In Fig. 2(a) we demonstrate a noteworthy discrepancy between the two techniques with regard to the identification of the gas-liquid interface. In more detail, the PLIF70 film-thickness measurement lies significantly and consistently above the BBLIF measurement (and also the PLIF90 trace). Close inspection of the presented PLIF frame also reveals a distinct bright line inside the illuminated flow-region, which overlaps the location of the gas-liquid interface obtained by application of BBLIF. If we assume that this line corresponds to the true location of the interface, then the "glowing" region above it is most likely related to the mirror effect described theoretically by Häber et al., (2015). According to their model, some of the light emitted by the illuminated liquid volume undergoes total internal reflection (TIR) at the gas-liquid interface, creating a false image of the film above the true image.

Based on our own ray-tracing calculations (see Fig. 3(a)), it becomes evident that both PLIF90, and especially PLIF70, are susceptible to overestimations of the film-thickness of flat films. Such overestimations, however, are not apparent in the mean film-thickness measurements obtained by PLIF (see, e.g., Zadrazil et al. (2014)); an observation that relates to two effects: (i) the averaging out of such local overestimations (applicable to smooth, flat films) by film regions where are more complex and "rough", and (ii) the (local) underestimation of the film thickness by PLIF (especially by PLIF90) due to refraction of the emitted light by the transverse (i.e., out-of-plane) curvature of the flow. Fast and slow ripples, as well as the disturbance waves themselves, are highly three-dimensional structures, (see, e.g., Cherdantsev et al. (2014)), and thus, this effect will be encountered and will affect the statistics of the PLIF-based film-thickness measurement. It should essentially be noted that as the observation angle is reduced (in this case from 90 ° to 70 °), this effect is suppressed, while the mirror effect is enhanced.

BBLIF is also sensitive to reflection errors, and progressively so as the in-plane and/or out-of-plane (due to wave three-dimensionality) slope of the interface increases with a nonlinear relation between the fluorescence intensity and the film thickness. In more detail, when the film surface is flat (or the interface slope is small) the reflection coefficient is $K \approx 0.02$, and any error in the measurement arising from the reflected light at the sloped interface is small. Note that the reflected contribution by a flat interface is already considered in Eq. 1 by the value of $K \approx 0.02$. When, however, the interface is at an angle to the incident light, the actual value of K will deviate from this value. In Fig. 3(b), we plot the reflection coefficient as a function of the incidence angle, and note that K starts to increase appreciably above $\theta = 30 – 35$ °, and until $\theta =$

48 °, which corresponds to the angle of total internal reflection. Specifically, *K* reaches a value of 0.06 at 40 °, 0.15 at 45 ° and 0.50 at 48 °, corresponding to average film thickness overestimates of around 5 %, 10 – 15 % and 40 – 50 %, which also depend on the local film thickness. Beyond 48 °, the light undergoes TIR and the contribution of the reflected beam becomes comparable, or even exceeds the primary emission (if the reflected light is focused locally by the curvilinear interface) leading to large overestimations of local film thickness.

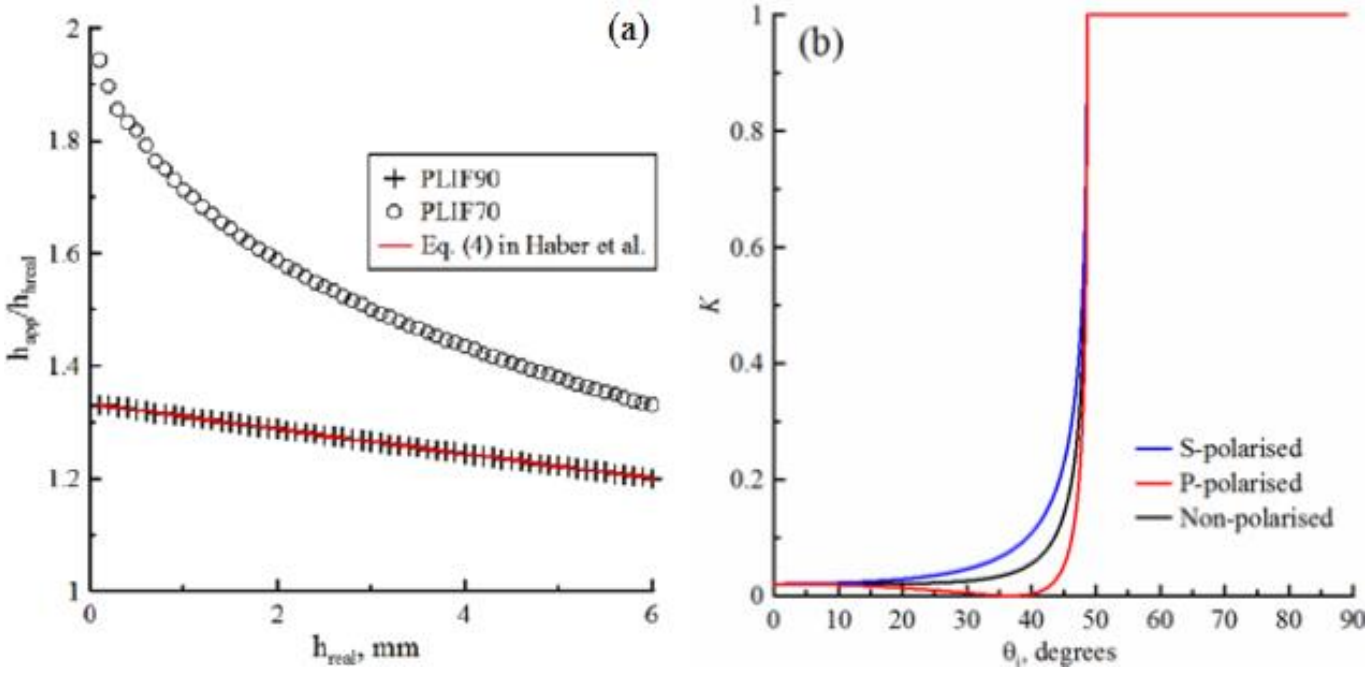


Fig. 3 (a) Plot of the film-thickness overestimation due to TIR for PLIF70 and PLIF90, as a function of the film thickness for a smooth and flat film. (b) Reflection coefficient at the water-air interface, *K*, plotted as a function of the incidence angle, θ_i, of the excitation light.

The occurrence of flow regions with steep slopes in smooth films is rare, and so errors of the aforementioned magnitude will not appear in average BBLIF film-thickness measurements due to averaging. However, the frequency of waves with significant curvature increases as the gas and liquid flow-rates increase. Examples of such cases are shown in Fig. 4, where bright regions are observed in raw BBLIF images, forming around transversely oriented lines that stem from the fronts of three-dimensional waves. These bright spots create localized, high-amplitude peaks in the film-thickness traces and conceal the true shape of the wave front in the excitation plane (which, in this case, it is assumed to track the bright line in the raw PLIF70 image).

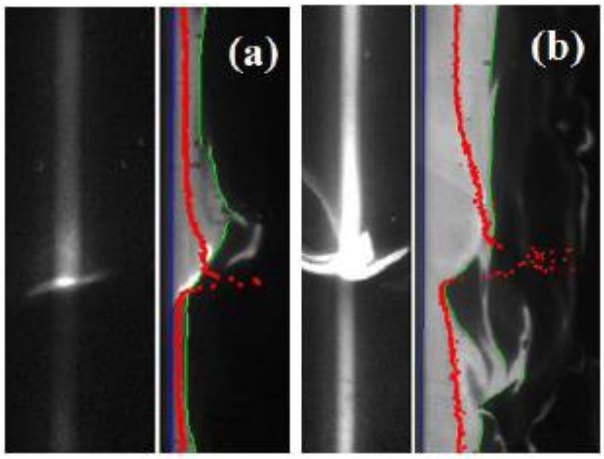


Fig. 4 Examples of overestimated film-thickness measurements by BBLIF at the fronts of waves observed in flows with: (a) Re_L = 150 and Re_G = 69,100, and (b) Re_L = 290 and Re_G = 41,200.

3.3. Rough films

In rough films, one expects to encounter all aforementioned error-sources; the overestimation of h_P due to TIR, the underestimation of h_P due to the 3-D nature of the waves, and the overestimation of h_{BB} due to interfacial reflections when the film slope increases. In Fig. 5, we show a number of BBLIF, PLIF90 and PLIF70 example frames from two experimental runs. In some case, although the BBLIF data contain numerous narrow peaks (appearing either at steep slopes or bubbles), between these peaks, the BBLIF data agree well with the PLIF70 data. This suggests that the mirror effect can be suppressed when the film roughness is high. At the same time, PLIF90 does not show agreement with BBLIF, in some cases yielding much lower film-thickness values along the disturbance waves. In particular, Fig. 5(c) and (d) show examples in which the rough surface of the disturbance waves is not reflected, and the film thickness corresponds to the base-film thickness.

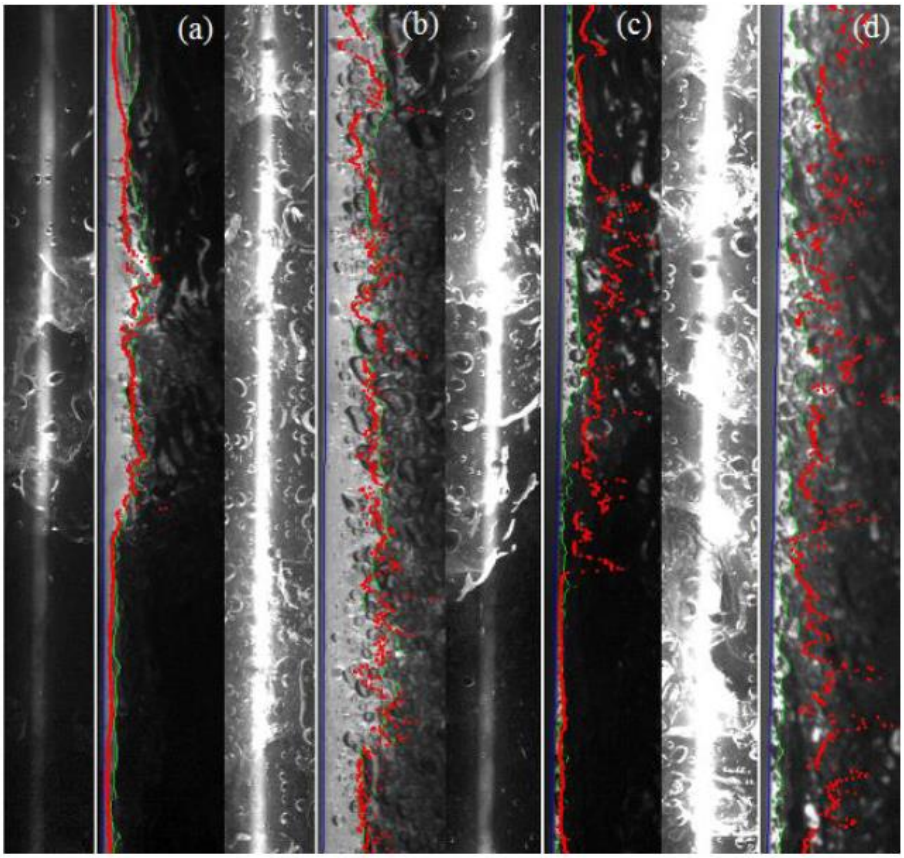


Fig. 5 Sample PLIF70 (a, b), PLIF90 (c, d) and BBLIF frames from flows with Re_L = 290, Re_G = 77,800 (a, c) and Re_L = 1,350, Re_G = 51,800 (b, d).

3.4. Direct comparison of the two techniques

The frame-by-frame comparison and related discussion performed above was aimed at providing us with an in-depth understanding of the error sources associated with each technique. We now proceed to compare film-thickness distributions obtained by each method, in order to assess the impact of these errors across the range of investigated flow conditions. In building these 2-D distributions, $N(h_P,h_{BB})$, each $\{t,x\}$-combination (i.e., each thickness measurement at time, t, and location, x, along the imaging domain) contributes a number N to a 2-D bin, with horizontal coordinates h_{BB} and vertical coordinates h_P. When presented in a graphical form (in Figs. 6 and 7), the brightness of each bin corresponds to the number of events it encompasses. In order to enhance the visibility of less probable $\{h_P,h_{BB}\}$ combinations, the 2-D histograms are presented with the brightness scaled as $\log2(N(h_P,h_{BB}))$. The blue lines mark the borders of regions encompassing 80 % and 90 % of the data points.

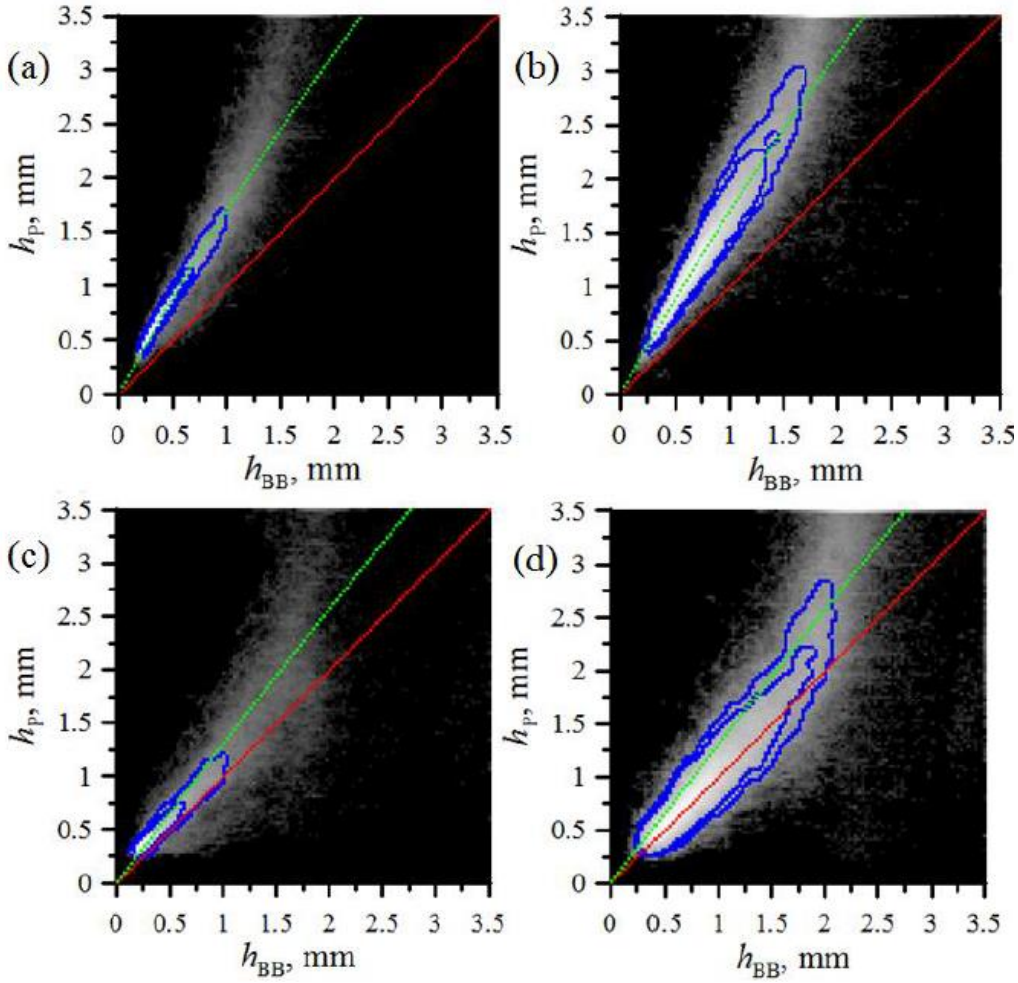


Fig. 6 Probability distributions compiled using PLIF70 (a, b), PLIF90 (c, d) and BBLIF data for flows with Re_L = 290 (a, c), Re_L = 1,350 (b, d) and Re_G = 0. The grayscale indicates the logarithm of the number of events, the red line corresponds to $h_P = h_{BB}$, and the green line shows the predicted film thickness based on the mirror effect.

In Fig. 6, we present 2-D distributions for both PLIF70 and PLIF90 in smooth films (with Re_G = 0), and for Re_L = 290 and Re_L = 1,350. In the first instance (i.e., for the PLIF70 data) the majority of the data points follow the predicted trend (see, Fig. 3) relating to the mirror effect, shown here by the green line. This observation provides additional evidence of the reliability of BBLIF in measuring smooth films, at least when the interface gradient is much smaller than the TIR angle. Regarding the PLIF90 results, the main body of data lies between the green and red lines (the latter representing $h_P = h_{BB}$). This observation can most probably be linked to the 3-D nature of the waves, which can reduce the mirror effect in PLIF but also refract the fluorescence emission (depending on the local curvature), effectively hiding the gas-liquid interface. Another interesting observation in Fig. 6 concerns the gradual deviation at thicker films, possibly due to the narrow laser sheet and large BBLIF measurement angle and/or signal saturation.

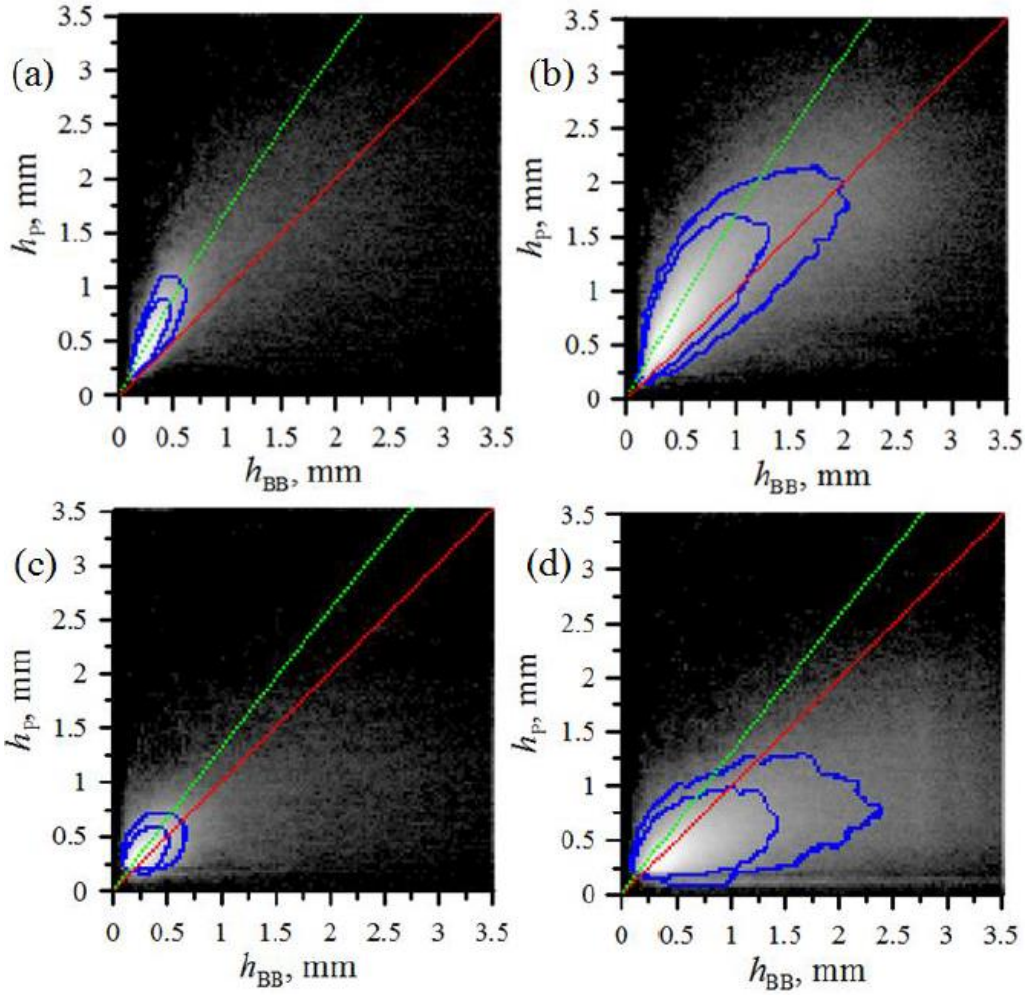


Fig. 7 Probability distributions compiled using PLIF70 (a, b), PLIF90 (c, d) and BBLIF data for flows with Re_L = 290 (a, c), Re_L = 1,350 (b, d) and Re_G = 51,800. The grayscale indicates the logarithm of the number of events, the red line corresponds to $h_P = h_{BB}$, and the green line shows the predicted film thickness based on the mirror effect.

In Fig. 7, we perform the same comparison as above in Fig. 6, this time, however, for rough films (i.e., in presence of strong shear). Close inspection of the PLIF70 results reveals that the presence of a rougher interface pushes the distribution towards lower h_P. Though the majority of the data points still group around the green line, a significant number approach the red line. This observation is in agreement with the previously noted suppression of the mirror effect at the highly 3-D surface of the disturbance waves. For PLIF90, the same effect is even more pronounced, with a significant portion of the data points lying well below the red line. This condition, which is also demonstrated in Fig. 5 (c, d), could be linked to underestimations of the true film thickness by PLIF90 in comparison to PLIF70, due to vulnerability of the former to three-dimensionality of

highly agitated film surface. Finally, as in Fig. 6, there is a gradual deviation at thicker films, however, here the overestimation of BBLIF due to reflections at the interface may be at play.

4. Conclusions

We have presented a comparative study of two advanced optical techniques that can provide detailed, quantitative, space- and time-resolved film-thickness measurement in downwards annular gas-liquid flows, namely planar laser-induced fluorescence (PLIF) and brightness-based laser-induced fluorescence (BBLIF). Both techniques employ the principle of laser-induced fluorescence, but differ in terms of the method used in each case to recover the local and instantaneous film thickness. In the present experiment campaign, the two techniques were applied simultaneously, using the same laser sheet for excitation of the fluorescent dye, and a pair of cameras that are arranged to image the same flow region. Aside from a direct comparison between PLIF and BBLIF, the effect of the observation angle, in the case of PLIF, is also examined; specifically, in addition to the "standard" configuration whereby the camera is positioned at a right angle to the laser sheet (PLIF90), a second configuration with the PLIF camera positioned at a 70 ° (PLIF70) angle to the excitation plane was also employed.

The main objective of this study is to identify and quantify the error sources associated with each technique. The "mirror effect", recently described by Häber et al. (2015), is the most prominent error source associated with PLIF. In the present work, we confirm its presence experimentally when the film surface is smooth, but note that in contrast to the prediction by Häber et al. (2015), the reflected intensity is sometimes marked by a bright line that appears in images inside the apparent liquid domain. The location of this line, agrees well with the film thickness measured by the BBLIF method, which is proven here to be a reliable method when measuring smooth and flat films (with free-surface angles up to ~40 – 45 ° to the horizontal). The predicted overestimation of film thickness in smooth films due to the mirror effect in PLIF is shown to be in good agreement to the experimentally measured ratio of the film thickness measured by PLIF to that measured by BBLIF. As the film surface becomes rougher, however, the mirror effect is suppressed in the PLIF images and the disparity between the two techniques is reduced. In addition to the mirror effect, PLIF is susceptible to underestimations of the local film-thickness owing to refraction at the three-dimensional fronts of waves. This effect is more prominent for PLIF90, but also acts to cancel out overestimations due to total internal reflection when the average film thickness is considered.

BBLIF is shown to produce reliable film-thickness measurements when the film surface is flat and smooth, with the total random error (for the present experiments) estimated at 10 %. When

the gas-shear velocity is increased substantially, the film surface becomes rough with significant curvature and the entrainment of bubbles in the liquid phases and droplets in the gas phases becomes significant. Under such conditions, it is found that BBLIF suffers from errors relating to reflections at the (curved and angled) interface, which become progressively worse as the total internal reflection is approached or exceeded. Furthermore, special attention needs to be paid in the experiment design stage to issues relating to the dynamic range of the measurement, the reduced measurement sensitivity and in avoiding possible signal saturation especially when measuring thicker films given the large variations in film thickness experienced in such flows.

Acknowledgement

This work was supported by the UK Engineering and Physical Sciences Research Council (EPSRC) [grant numbers EP/K008595/1 and EP/L020564/1], and by the Royal Society and the UK Department for International Development (DFID) [Africa Capacity Building Initiative].

References

Adomeit P, Renz U (2000) Hydrodynamics of three-dimensional waves in laminar falling films. Int J Multiph Flow 26: 1183-1208.

Alekseenko SV, Antipin VA, Guzanov VV, Kharlamov SM, Markovich DM (2005) Three-dimensional solitary waves on falling liquid film at low Reynolds numbers. Phys Fluids, doi: 10.1063/1.2158428.

Alekseenko SV, Antipin VA, Cherdantsev AV, Kharlamov SM, Markovich DM (2009) Two-wave structure of liquid film and waves interrelation in annular gas-liquid flow with and without entrainment. Phys Fluids 21: 061701-061704.

Alekseenko SV, Cherdantsev AV, Heinz OM, Kharlamov SM, Markovich DM (2014) Analysis of spatial and temporal evolution of disturbance waves and ripples in annular gas-liquid flow. Int J Multiph Flow, 67: 122–134.

Belt RJ, Van't Westende JMC, Prasser HM, Portela LM (2010) Time and spatially resolved measurements of interfacial waves in vertical annular flow. Int J Multiph Flow 36: 570–587.

Charogiannis A, An JS, Markides CN (2015) A simultaneous planar laser-induced fluorescence, particle image velocimetry and particle tracking velocimetry technique for the investigation of thin liquid-film flows. Exp Therm Fluid Sci, 68: 516–536.

Charogiannis A, Denner F, van Wachem BGM, Kalliadasis, S, Markides CN (2017) Detailed hydrodynamic characterization of harmonically excited falling-film flows: A combined experimental and computational study, Phys Rev Fluids 2: 014002-1–37.

Cherdantsev AV, Hann DB, Azzopardi BJ (2014) Study of gas-sheared liquid film in horizontal rectangular duct using high-speed LIF technique: three-dimensional wavy structure and its relation to liquid entrainment. Int J Multiph Flow 67: 52–64.

Cherdantsev AV, Hann DB, Hewakandamby BN, Azzopardi BJ (2017) Study of the impacts of droplets deposited from the gas core onto a gas-sheared liquid film. Int J Multiph Flow, 88: 69–86.

Chu KJ, Dukler AE (1974) Statistical characteristics of thin, wavy films: Part II. Studies of the substrate and its wave structure. AIChE J. 20: 695–706.

Farias PSC, Martins FJWA, Sampaio LEB, Serfaty R, Azevedo LFA (2012) Liquid film characterization in horizontal, annular, two-phase, gas–liquid flow using time-resolved laser-induced fluorescence. Exp Fluids 52: 633–645.

Häber T, Gebretsadik M, Bockhorn H, Zarzalis N (2015) The effect of total reflection in PLIF imaging of annular thin films. Int J Multiph Flow 76: 64–72.

Han H, Zhu Z, Gabriel K (2006) A study on the effect of gas flow rate on the wave characteristics in two-phase gas–liquid annular flow. Nucl Eng Des 236: 2580–2588.

Hazuku T, Takamasa T, Matsumoto Y (2008) Experimental study on axial development of liquid film in vertical upward annular two-phase flow. Int J Multiph Flow 34: 111–127.

Hewitt GF, Lovegrove PC, Nicholls B (1964) Film thickness measurement using a fluorescence technique I: Description of the method. AERE-R4478, Harwell, UKAEA.

Karapantsios TD, Paras SV, Karabelas AJ (1989) Statistical characteristics of free falling films at high Reynolds numbers. Int J Multiph Flow 15(1): 1–21.

Kharlamov SM, Guzanov VV, Bobylev AV, Alekseenko SV, Markovich DM (2015) The transition from two-dimensional to three-dimensional waves in falling liquid films: Wave patterns and transverse redistribution of local flow rates. Phys Fluids 27: 114106.

Liu J, Paul JD, Gollub JP (1993) Measurements of the primary instabilities of film flows. J Fluid Mech 250: 69–101.

Pham SH, Kawara Z, Yokomine T, Kunugi T (2014) Detailed observations of wavy interface behaviors of annular two-phase flow on rod bundle geometry. Int J Multiph Flow 59: 135–144.

Schubring D, Ashwood AC, Shedd TA, Hurlburt ET (2010) Planar laser-induced fluorescence (PLIF) measurements of liquid film thickness in annular flow. Part I: Methods and data. Int J Multiph Flow 36: 815–824.

Webb D, Hewitt GF (1975) Downwards co-current annular flow. Int J Multiph Flow 2: 35–49.

Woodmansee DE, Hanratty TJ (1969) Mechanism for the removal of droplets from a liquid surface by a parallel air flow. Chem Eng Sci 24: 299-307.

Zadrazil I, Matar OK, Markides CN (2014) An experimental characterization of downwards gas–liquid annular flow by laser-induced fluorescence: Flow regimes and film statistics. Int J Multiph Flow 60: 87–102.

Zadrazil I, Markides CN (2014) An experimental characterization of liquid films in downwards co-current gas–liquid annular flow by particle image and tracking velocimetry. Int J Multiph Flow 67: 42–53.

Zhao Y, Markides CN, Matar OK, Hewitt GF (2013) Disturbance wave development in two-phase gas–liquid upwards vertical annular flow. Int J Multiph Flow 55: 111–129.

View publication stats